Photo-Induced Pyridine Substitution in cis-[Ru(bpy)2(py)2]Cl2: A Snapshot by Time-Resolved X-ray Solution Scattering

Photo-induced Pyridine Substitution in *cis*-$[Ru(bpy)_2(py)_2]Cl_2$: A Snapshot by Time-resolved X-ray Solution Scattering

Luca Salassa,[†,‡] Elisa Borfecchia,[†] Tiziana Ruiu,[†] Claudio Garino,[†] Diego Gianolio,[†] Roberto Gobetto,[†] Peter J. Sadler,[‡] Marco Cammarata,[§*] Michael Wulff,[§] and Carlo Lamberti[*,†]

Dipartimento di Chimica I.F.M., NIS Centro di Eccellenza e INSTM Centro di Riferimento, Università di Torino, Via P. Giuria 7, I-10125 Torino, Italy, Department of Chemistry, University of Warwick, Gibbet Hill Rd, Coventry CV4 7AL, United Kingdom, and European Synchrotron Radiation Facility, 6 rue Jules Horowitz, BP220, F-38043, Grenoble CEDEX, France

Email: carlo.lamberti@unito.it

[†] Dipartimento di Chimica I.F.M., NIS Centro di Eccellenza e INSTM Centro di Riferimento.

[‡] Department of Chemistry.

[§] European Synchrotron Radiation Facility.

[*] Current address: SLAC National Accelerator Laboratory, 2575 Sand Hill Road, 94025, Menlo Park, CA, USA

Keywords: photochemistry - anticancer - X-ray scattering - ruthenium - time-resolved

Abstract

Determination of transient structures in light-induced processes is a challenging goal for time-resolved techniques. Such techniques are becoming successful in detecting ultrafast structural changes in molecules and do not require the presence of probe-like groups. Here, we demonstrate that TR-WAXS (Time-Resolved Wide Angle X-ray Scattering) can be successfully employed to study the photochemistry of *cis*-$[Ru(bpy)_2(py)_2]Cl_2$, a mononuclear ruthenium complex of interest in the field of photoactivatable anticancer agents. TR-WAXS is able to detect the release of a pyridine ligand and the coordination of a solvent molecule on a faster time-scale than 800 ns of laser excitation. The direct measurement of the photodissociation of pyridine is a major advance in the field of time-resolved techniques allowing detection, for the first time, of the release of a multiatomic ligand formed by low Z atoms. These data demonstrate that TR-WAXS is a powerful technique for studying rapid ligand substitution processes involving photoactive metal complexes of biological interest.

1. Introduction

The unique photophysical and photochemical properties of metal-diimine complexes have been successfully exploited in numerous medical[1-4] and technological[5-9] applications. Among these, we are currently exploring the possibility of developing photoactivatable Ru-diimine anticancer agents[10-12] which can be selectively activated in cancer cells by light. When irradiated, such complexes can undergo ligand dissociation and subsequent coordination of a solvent (water) molecule. The aqua derivative formed is highly reactive and can interact with target macromolecules leading to cell death (Scheme 1).

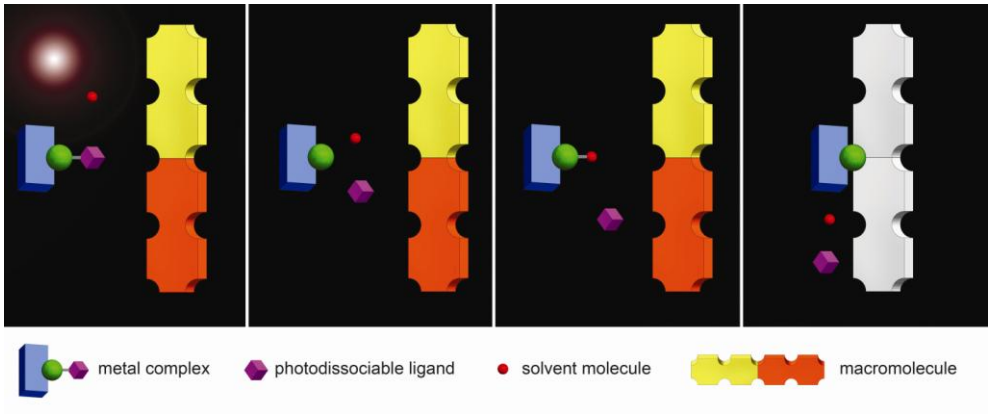

Scheme 1. A photoactivation pathway for metal-based anticancer drugs.

The potential of these derivatives as cytotoxic agents is dependent on their excited-state features which control, for example, the absorption properties of photoactivatable metal complexes and the nature of their photoreaction intermediates and photoproducts.[4,13-18] Obtaining structural information on transient species generated by light excitation is therefore crucial to the field of photoactivatable metal-based anticancer agents. It can reveal the mechanism of activation of the 'prodrug' helping to understand the overall mechanism of action of the metal complex in cells. Moreover, experimental determination of transient structures can be used to validate computational methods which are accessible and powerful tools for studying the photochemistry of anticancer agents and improving their rational design.[10,19]

In the last few years, time-resolved XAS (X-ray Absorption Spectroscopy) has been successfully employed for studying excited-state structures in solution, as demonstrated by the work of several authors.[20-25] Direct observation of structural dynamics with atomic resolution can be also obtained by TR-WAXS (Time-Resolved Wide Angle X-ray Scattering). This young technique has been used to characterize light-induced structural changes in solution for a variety of systems ranging from diatomic molecules[26] to large biomolecules.[27] TR-WAXS can capture, in one radial dimension, all the transient structures present in the laser-irradiated volume by collecting X-ray

scattering patterns as a function of time delay. Data analysis of the diffraction patterns can then reveal the structural evolution of different reaction pathways, limited only by the signal-to-noise ratio of the difference signal between excited and non-excited states. Unfortunately, this has so far mainly limited the use of TR-WAXS to the study of light-induced structural dynamics for molecules containing heavy atoms. For example, TR-WAXS has succeeded in monitoring the photochemistry of CHI_3[28] and HgI_2[29] both of which can dissociate one or two I (Z = 53) atoms on the sub-μs timescale. In these examples and others,[28,30-32] the heavy iodine atom has the role of ensuring a sufficient scattering signal from the photochemically active solute molecule. This helps with extraction of the contribution of the solute photochemistry from the whole diffraction signal, which contains also all solvent-related terms (solute-solvent and solvent-solvent).

A challenge for this emerging technique is to extend its use to detect photoprocesses involving the release of complex fragments formed by low Z atoms such as C, N and O (Z = 6, 7 and 8, respectively). This will provide a significant increase in the variety of molecules that can be studied with TR-WAXS.

Herein we report a direct observation by TR-WAXS of light-induced ligand dissociation from a mononuclear metal complex of interest in the field of photochemotherapeutic agents, namely *cis*-$[Ru(bpy)_2(py)_2]Cl_2$ (bpy = 2,2′-bipyridine and py = pyridine). Upon excitation of the metal-to-ligand charge-transfer (^{1}MLCT) band centered at 460 nm in the absorption spectrum, this model compound efficiently releases (photodissociation yield ϕ = 0.2)[33] one pyridine ligand and subsequently coordinates a solvent molecule (Scheme 2).

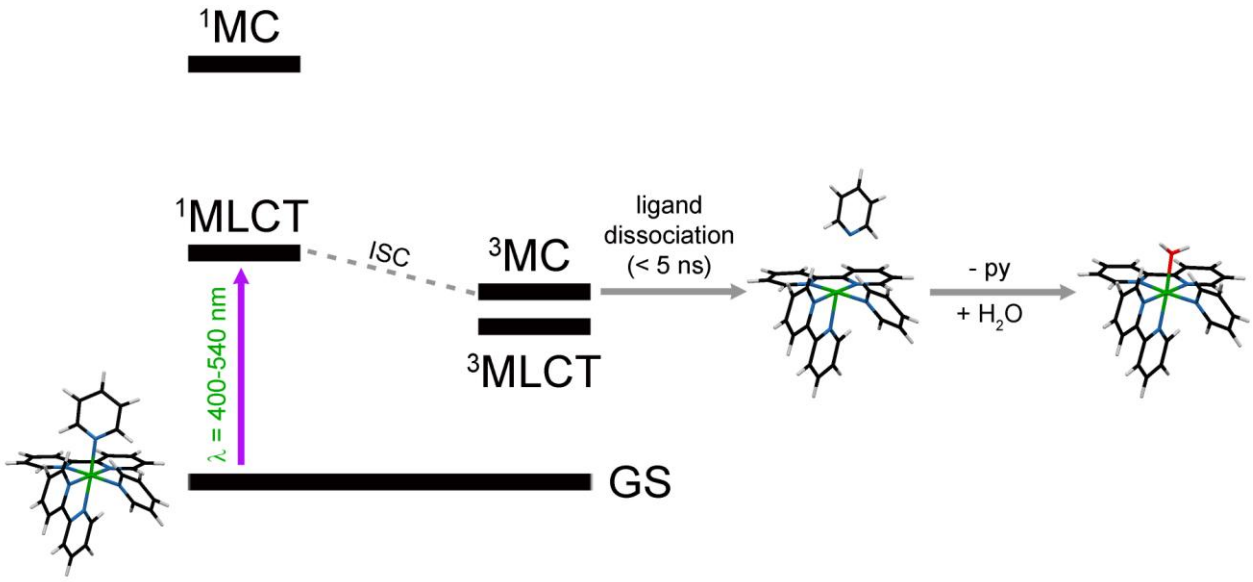

Scheme 2. Photodissociation scheme for *cis*-$[Ru(bpy)_2(py)_2]^{2+}$.

We show here that TR-WAXS is able to capture in the scattering images the release of the pyridine ligand from the metal centre and the subsequent coordination of a water molecule within 800 ns from laser excitation (the shortest time-delay acquired). The experiment provides a snapshot of the final stage of the ruthenium complex photodissociation. TR-WAXS captures two molecular events, the release of py and the coordination of an H_2O molecule, and records them as a function of the inter-atomic radial distribution function. The TR-WAXS signal is extracted as the difference between the scattering profile before and after laser excitation. Consequently, the technique detects the differences in the radial distribution function between the un-reacted and the reacted states.

The structural information in our TR-WAXS experiment is unprecedented and shows that the technique can be successfully used to monitor the photorelease of a heterocyclic fragment formed by low Z atoms. Interestingly, information on second and third shell[34] atoms around the metal center is also obtained. This result is even more remarkable if the small difference in the diffraction signal of the reacted and un-reacted metal complex is considered.

The sub-μs temporal resolution of the experiment is determined by the choice of the excitation method (see the Results and Discussion section), and still needs to be improved to capture the excited-state dynamics of the py release from *cis*-$[Ru(bpy)_2(py)_2]Cl_2$ (1–10 ns) and the water coordination that follows. Nevertheless, the results reported here establish TR-WAXS as a new tool for the study of photoactive metal complexes. We demonstrate how TR-WAXS can probe bond cleavage between the Ru center and the low Z atoms of the leaving pyridine ligand, as well as the formation of a new Ru–O bond due to the coordination of a solvent molecule.

In the field of metal-based anticancer agents, TR-WAXS structural determination of short-lived transient species generated from such systems (e.g. under physiological conditions) could lead to new discoveries about their mechanism of action.

2. Experimental Section

2.1. Sample preparation. *cis*-$[Ru(bpy)_2(py)_2](ClO_4)_2$ was synthesized according to the literature procedure.[35] To increase its water solubility, the chloride derivative *cis*-$[Ru(bpy)_2(py)_2]Cl_2$ was prepared by anion exchange of a methanol solution of *cis*-$[Ru(bpy)_2(py)_2](ClO_4)_2$ on a Dowex weakly basic anion exchanger resin (purchased from Aldrich). The 20 mM solution of *cis*-$[Ru(bpy)_2(py)_2]Cl_2$ was prepared dissolving 5.14 g (8.00 mmol) of the complex in 400 ml of water.

2.2. Computational details. All geometry optimization calculations were performed with the Gaussian 03[36] (G03) program package employing the DFT method with the Becke's three-parameter hybrid functional[37] and the Lee-Yang-Parr's gradient corrected correlation functional[38]

(B3LYP). The LanL2DZ basis set and effective core potential[39] were used for the Ru atom and the split-valence 6-311G** basis set[40] was applied for all other atoms in **M1** and **M2**, while the 3-21G** basis set was employed in **M3** (see Results and Discussion section, 3.2. TR-WAXS measurements). In **M3**, the structure of the photoproduct *cis*-$[Ru(bpy)_2(py)(H_2O)]^{2+}$ was optimized by adding three explicit water molecules in proximity of the coordinated water to simulate the solvent effect. The conductor-like polarizable continuum model method (CPCM)[41-43] with water as solvent was used to take into account the solvent effect. The nature of all stationary points was confirmed by normal-mode analysis.

2.3. EXAFS data collection and data analysis. X-ray absorption experiments, at the Ru K-edge (22117 eV), were performed at the BM26A of the ESRF facility (Grenoble, F).[44] The white beam was monochromatized using a Si(111) double crystal; harmonic rejection was achieved by using Pt-coated Si mirrors. An EXAFS cell, specifically devoted to liquid samples, was filled with a 50 mM aqueous solution of *cis*-$[Ru(bpy)_2(py)_2]Cl_2$. Due to low concentration of complex, EXAFS spectra were acquired in fluorescence mode, by means of a 9-element germanium monolithic detector, collecting the Ru $K_{\alpha 1-3}$ fluorescence lines in the 18500–19500 eV range. The intensity of the incident beam was monitored by an ionization chamber. The pre-edge region and XANES part of the spectra were acquired with a constant energy step of 10 and 1.3 eV respectively, while the EXAFS part (from k = 2 $Å^{-1}$ up to 14 $Å^{-1}$) was collected with a $\Delta k = 0.05$ $Å^{-1}$, resulting in a variable sampling step in energy. The integration time per point was 2 s for the pre-edge region, 5 s in the XANES region, and linearly variable from 5 to 30 s in the EXAFS part of the spectrum.

The extraction of the $\chi(k)$ function was performed using Athena programs.[45] Three consecutive EXAFS spectra were collected, resulting in three $\mu(x)$ spectra being obtained by integrating the counts of the 9 elements of the fluorescence detector. Corresponding k^3-weighted $\chi(k)$ functions were averaged and Fourier Transformed in the Δk = 2.00–14.00 $Å^{-1}$ interval. The quality of the averaged $k^3\chi(k)$ data can be appreciated in Figure 1a. EXAFS data analysis was performed using the Arthemis software.[45] The fits were performed in R-space in the ΔR = 1.00–5.00 Å range ($2\Delta k\Delta R/\pi \sim 30$). Phase and amplitude functions of each path were calculated by FEFF8.4 code[46] using the structure obtained from DFT calculations as input (B3LYP/LanL2DZ/6-311G**). Due to the complexity of the structure, more than 200 single scattering (SS) and multiple scattering (MS) paths are generated by the code. According to the criteria described in the Supporting Information, we selected 30 main paths that were sufficient to reconstruct the overall EXAFS signal. To limit the number of optimized variables, all paths were optimized with the same amplitude factor (S_0^2) and with the same energy shift (ΔE) parameter. Moreover, both the two py and two bpy ligands were

considered as rigid molecules whose only degree of freedom is the radial translation along the corresponding Ru–N axis. The two pyridine ligands were assumed to behave in the same way and the same action was inferred for the two bpy ligands as well. Consequently, the only two structural parameters optimized in the fit were the distances $R_{Ru–N(py)}$ and $R_{Ru–N(bpy)}$; the lengths of all the other paths were calculated starting from these two values, according to geometrical constraints imposed by the rigidity of the py and bpy ligands. Concerning the Debye-Waller (DW) factors, only two parameters were optimized: $\sigma_{Ru–N(py)}$ and $\sigma_{Ru–N(bpy)}$, associated with Ru–N bonds for py or bpy ligands, respectively. For SS and MS paths involving atoms of the same ligand, we imposed the corresponding DW factor to be $\sigma^2 = \sigma^2_{Ru–N(L)} \sqrt{(R_{eff}/R_{Ru–N(L)})}$ (L = py or bpy). In this way, when the mean free path length (R_{eff}) increases, we roughly take into account the expected proportional expansion of its standard deviation (σ). Several almost co-linear MS paths involve two N atoms of two opposite L and L' ligands. In these cases their DW factors were computed as $\sigma^2_{MS} = [\sigma_{Ru–N(L)} + \sigma_{Ru–N(L')}]^2$. Summarizing, the fit runs over 6 independent parameters only. A similar approach to validating a complex structure by EXAFS (known by XRD or by ab initio calculations), maintaining a limited number of optimized parameters, has already been successfully employed in the case of $[Ru(bpy)_n(AP)_{6–2n}]Cl_2$ (AP = 4-aminopyridine, n = 1, 2, 3),[11,47] of $CrCp_2$ (Cp = cyclopentadienyl) hosted in different porous matrices,[48,49] and metal organic frameworks.[50-52]

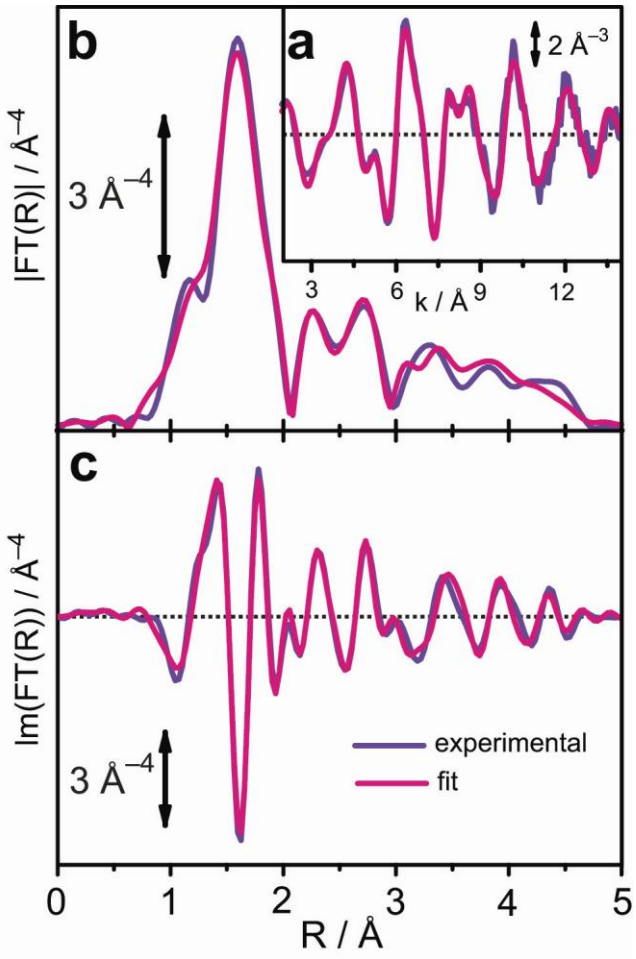

Figure 1. **a)** Experimental $k^3\chi(k)$ EXAFS spectrum of *cis*-$[Ru(bpy)_2(py)_2]Cl_2$ (violet curve) compared with its best fit (magenta curve). **b)** Corresponding phase uncorrected FT modulus and **c)** imaginary part. Optimized parameters of the fit are reported in Table 1.

2.4. TR-WAXS data collection. A full account on the ID09B beamline architecture and instrumentation is provided elsewhere.[53] The sample solution was continuously circulated using a liquid jet apparatus. The liquid enters from above and is collected in a funnel below the interaction point. The pumping speed of the circulating solution is set such that the sample is replaced between two laser pulses (ca. 1 ms apart) and to guarantee a laminar regime of the falling liquid, necessary to maintain a constant sample thickness crossed by the pumping and probing beam. The scattering pattern is collected on a CCD detector centered on the incident beam. A Photonics Industries Laser "DM50" was used to photoexcite the sample. The laser repetition rate was identical to that of the X-rays (~ 986 Hz). Using a diode current of 8.6 A, a 800 ns pulse was obtained. The laser energy on the sample was 195 mW and a transmission (through the sample) of about 60% was measured. The laser beam was focus to 0.37 × 0.19 (hor × ver) mm^2. The estimated percentage of photodissociated molecules per laser pulse is ca. 6% in the irradiated volume (2.7×10^{-2} mm^3) (see Supporting Information).[21] We benefited from the new fast readout FReLoN CCD detector. The raw images were corrected in order to take into account several unavoidable effects: i) pixel/optical fibers

connection; ii) fluorescent screen non-homogeneity; iii) X-ray beam polarization (in plane, linear)[26,54-57]; iv) X-ray to visible photon conversion efficiency due to the θ-dependence of the optical path through the fluorescent screen; v) X-ray extinction due to sample absorption (θ-dependent because of the path length). Afterwards, the azimuthal averaging procedure was performed, to obtain the I(θ) and thus I(q) curves using the peak of the narrow λ distribution of the spectrum emitted by the U17 undulator. This procedure was repeated for each time delay τ. Differential $\Delta I(q, \tau) = I(q, \tau) - I(q, \tau_0 = -1200\ ns)$ curves were calculated between adjacent acquisitions and then averaged over 530 acquisitions as reported in Figure 2c.

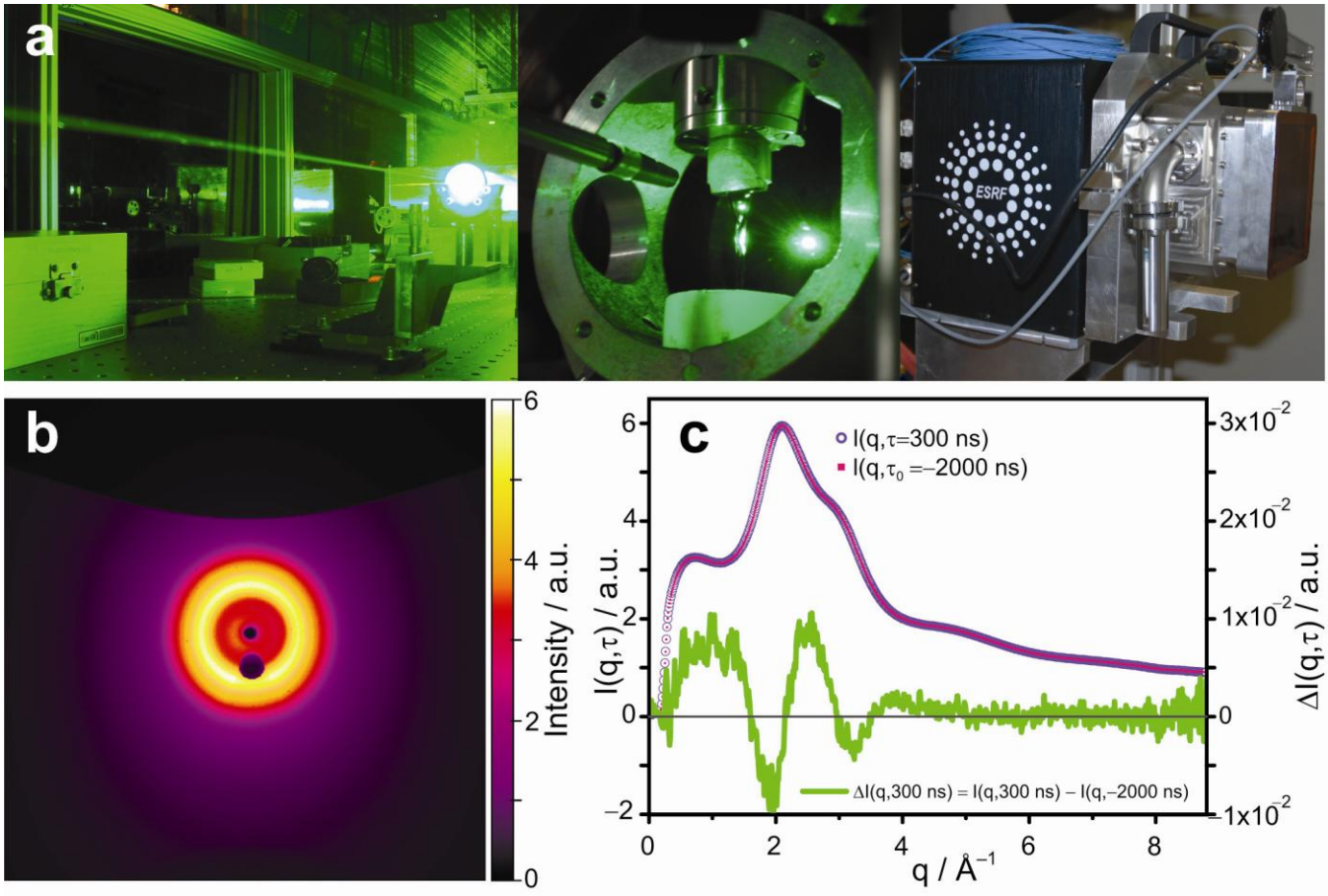

Figure 2. Experimental setup and raw data collection. **a)** Experimental setup. From left to right: optical bench operating with a λ = 532 nm laser (pulse length 800 ns); liquid-jet cell; FReLoN 2D CCD detector. **b)** 2D X-ray scattering image from the FReLoN 2D CCD detector, collected with positive time delay between pump and probe of τ = 800 ns. The top (large) and the bottom (small) dark parts are the shadows from the nozzle in the liquid-jet cell (see part (**a**), central picture). The two dark circles are due to the X-ray and laser beam-stops needed to protect the CCD camera. **c)** Left ordinate axis: superimposition of I(q, τ = 800 ns) and I(q, τ_0 = –1200 ns) curves (open violet circles and pink dots, respectively) both obtained by azimuthal averaging of the single 2D image similar to that shown in part (**b**). Right ordinate axis: difference signal $\Delta I(q, \tau = 800\ ns) = I(q, \tau = 800\ ns) - I(q, \tau_0 = -1200\ ns)$, green curve.

3. Results and Discussion

3.1. Structure refinement of *cis*-[Ru(bpy)$_2$(py)$_2$]Cl$_2$ in aqueous solution by EXAFS spectroscopy. The EXAFS spectrum was simulated starting from the DFT-optimized geometry of *cis*-[Ru(bpy)$_2$(py)$_2$]Cl$_2$. The quality of the obtained fit in both R- and k-spaces can be appreciated in

Figure 1 and is further confirmed by the very low values of both R-factor and errors associated to the fitting parameters (see Table 1). It is worth highlighting that bpy units contribute to the high distance paths almost twice as much as the py units. Therefore, distances and Debye-Waller factors were determined with a better precision for the bpy ligands. Accordingly to the lower mass, py units of the complex exhibit a Debye-Waller factor higher than bpy. The nitrogen atom of the py units is located at a distance of 2.09 ± 0.01 Å from Ru, hence 0.08 Å shorter than the value predicted by DFT calculations (Table 1). Also the experimental Ru–N(bpy) distances are 0.03 Å shorter than the theoretical ones. Curiously, the optimized $R_{Ru–N(bpy)}$ and $R_{Ru–N(py)}$ distances become equivalent taking account of the associated errors. This behavior seems to be typical of the EXAFS technique; when several neighbors of the same chemical nature are located at close distances, there is a tendency to allow such distances to converge to a common value.[11,47,50] The higher correlation among parameters occurs for $R_{Ru–N(py)}/R_{Ru–N(bpy)} = –0.73$. All other correlations are below 0.5 in absolute value. Summarizing, we conclude that EXAFS data analysis fully confirms the overall structure optimized in the DFT calculations. The results reported in Table 1 are in good agreement with previous studies performed on similar ruthenium complexes.[11,47] (For more details regarding the most relevant paths contributing to the EXAFS signal, see Supporting Information).

Table 1. Summary of the optimized parameters in the EXAFS data fitting (Figure 1). The fits were performed in R-space in the 1.0–5.0 Å range over k^3-weighted FT of the $\chi(k)$ functions performed in the 2.0–14.0 $Å^{-1}$ interval. A single ΔE_0 and a single S_0^2 were optimized for all SS and MS paths. Optimized bond distances are compared to the average values obtained from DFT calculations.

	cis-$[Ru(bpy)_2(py)_2]Cl_2$	
parameters	**EXAFS**	**DFT**
N_{ind}	30	-
N_{fit}	6	-
R_{factor}	0.032	-
S_0^2	0.72 ± 0.05	-
ΔE (eV)	2.5 ± 0.6	-
$R_{Ru–N(bpy)}$ (Å)	2.073 ± 0.007	2.112
$\sigma_{Ru–N(bpy)}$ ($Å^2$)	0.0027 ± 0.0006	-
$R_{Ru–N(py)}$ (Å)	2.09 ± 0.01	2.172
$\sigma_{Ru–N(py)}$ ($Å^2$)	0.004 ± 0.001	-

3.2. TR-WAXS measurement. TR-WAXS experiments on *cis*-$[Ru(bpy)_2(py)_2]Cl_2$ were performed at the European Synchrotron Radiation Facility (ESRF) on the ID09B beamline,[53] which offers a unique setup for ultrafast pump-and-probe experiments (Supporting Information).

All the data were collected using a 20 mM aqueous solution of *cis*-$[Ru(bpy)_2(py)_2]Cl_2$ and excitation, with an 800 ns-long pulse of 532 nm light, in the red tail of the ^{1}MLCT band in the visible part of the absorption spectrum. *Cis*-$[Ru(bpy)_2(py)_2]Cl_2$ does not show any emission in

aqueous solution at 298 K, nevertheless variable-temperature studies showed that emission (λ_{max} ~ 630 nm) from the ^{3}MLCT of the complex can occur at lower temperature (< 248 K) in an ethanol/methanol solution. The extrapolated emission lifetime at 298 K for the same solution is 2.7 ns,[58] in agreement with the value of 5 ns measured by Meyer *et al.* in dichloromethane at 298 K (λ_{max} ~ 630 nm, quantum yield < 0.0001).[59] The lack of emission in aqueous solution of the complex is due to a low-lying ^{3}MC (metal-centered) or ^{3}LF (ligand-field) state, which deactivates the ^{3}MLCT state and is also responsible for the py dissociation.[10]

The relatively long laser pulse was used to enhance the fraction of excited molecules thus increasing the difference signal. 2D diffraction images were taken at four different positive time delays (τ= 800, 1000, 1500 and 5500 ns) between laser-pump and X-ray-probe and then azimuthal-averaged to give the corresponding I(q, τ) curves.[26] Laser source features and the time delays were selected to allow exploration of TR-WAXS for *cis*-$[Ru(bpy)_2(py)_2]Cl_2$, considering both its structural and photochemical properties and the long acquisition time required to obtain a good signal-to-noise ratio. Excited-state structural changes were lost using the chosen excitation method since the reactive state has a much shorter lifetime compared to the laser pulse length. Instead, a quasi steady-state population of photochemically modified molecules was obtained and the changes in the structure of *cis*-$[Ru(bpy)_2(py)_2]Cl_2$ were captured by measuring the variation in scattering intensity. Thus, a structural snapshot of the photoproduct *cis*-$[Ru(bpy)_2(py)(H_2O)]^{2+}$ is taken simultaneously with the footprint left by the released pyridine fragment. A negative time delay τ_0 = –1200 ns was used to collect diffraction images as reference for the ground-state structure of *cis*-$[Ru(bpy)_2(py)_2]Cl_2$. This non-excited image is necessary in TR-WAXS to determine structural changes upon irradiation, since the technique relies on the difference between the X-ray scattering signal of the sample after (positive delays) and before (negative delay) laser irradiation. Therefore, differential intensities were defined as $\Delta I(q, \tau) = I(q, \tau) - I(q, \tau_0)$. Due to the very low signal-to-noise ratio of a single $\Delta I(q, \tau)$, whose magnitude is < 0.1% of the single I(q, τ) acquisition, 530 images for each time delay were collected and the corresponding $\Delta I(q, \tau)$ were averaged, giving a significant improvement in the signal-to-noise ratio (Figure 3a). At this stage in the data processing, measurements resulted in four identical curves, within the signal-to-noise ratio, indicating that the photochemical process was already complete after 800 ns (as expected). All the acquired data were then further averaged to improve the signal-to-noise ratio (see $\Delta I(q)$ green curve in Figure 3b). The q-weighted Fourier Transform (FT) of $\Delta I(q)$ resulted in $\Delta I(r)$ (see green curve in Figure 3c) which represents the difference in the overall radial distribution function of all components in the sample, after and before photoexcitation (solvent, metal complex and its fragments).

An important contribution to $\Delta I(r)$ is the solvent response to the heat-release from the solute molecules excited by the laser pulse.[60] In particular, due to the limiting dissociation yield (20%)[33] and the use of the long laser pulse to generate multiple chances of dissociation, we expect the solvent response to play an important role. Accurate extraction of the solvent contribution $\Delta I_{solv}(q)$ and its corresponding $\Delta I_{solv}(r)$ (black curves in Figure 3b and 3c) from the averaged $\Delta I(q)$ curve was therefore investigated. This was achieved by performing the same data acquisitions, but with the Ru sample replaced by a solution containing a phochemically-inert solute ($KMnO_4$) able to transfer a similar amount of heat to the solvent per laser pulse. This heat-removal procedure is critical for the present system, since only a small fraction of the solute reaches the photoactive excited state per laser-pulse and the information relevant to the structural changes in the molecule is very difficult to isolate from the total signal. The thermal relaxation decay time was estimated to be ca. 250 μs using the method of Fader.[61] Since this value is greater than time-scale of the TR-WAXS experiment, a contribution from the decay of thermal effects is not present in the TR-WAXS curves. The $\Delta I_{solv}(q)$ curve was scaled (scaling factor of 1.5) to minimize the difference between $\Delta I(q)$ and $\Delta I_{solv}(q)$ in the region 1.5 $Å^{-1}$–2.95 $Å^{-1}$, where the signal is dominated by the thermal rearrangement effects of the bulk water structure (Supporting Information). The scaled $\Delta I_{solv}(q)$ was thus subtracted from the overall signal $\Delta I(q)$, to give the difference $\Delta[\Delta I(q)] = \Delta I(q) - \Delta I_{solv}(q)$ (bottom purple curve in Figure 3b) which, despite being slightly noisy, exhibits well defined maxima and minima. In r-space the differences between $\Delta I(r)$ and $\Delta I_{solv}(r)$ are appreciable up to 5 Å, and result in a nicely structured $\Delta[\Delta I(r)]$ curve (bottom purple line in Figure 3c).

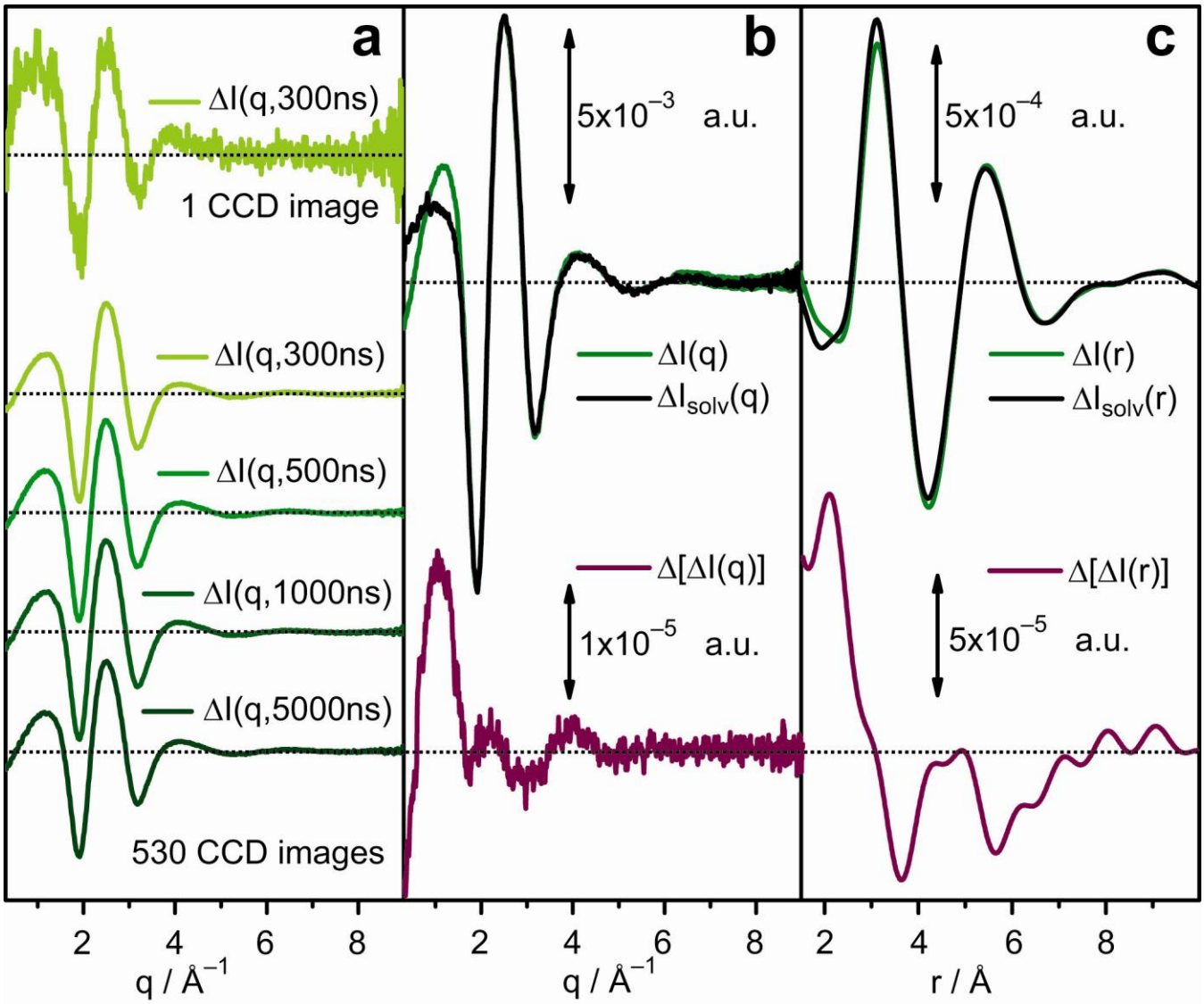

Figure 3. Experimental data. **a)** Differential intensities for *cis*-$[Ru(bpy)_2(py)_2]Cl_2$ in aqueous solution defined as $\Delta I(q, \tau) = I(q, \tau) - I(q, \tau_0)$, where $I(q, \tau)$ are signals collected at different time delays (τ = 800, 1000, 1500, 5500 ns) and $I(q, \tau_0)$ is the non-excited reference for the system before laser excitation. Top curve is obtained from a single acquisition at τ = 800 ns; the other curves are averaged over 530 CCD images. **b)** Top: comparison between averaging the four $\Delta I(q, \tau)$ curves reported in part (**a**) and the data obtained repeating the same experiment using $KMnO_4$ as photochemically inert solute. Bottom: difference between the two $\Delta I(q)$ curves reported in the top part. **c)** Top: $\Delta I(r)$ curves, obtained from q-weighted FT (in 0–9 $Å^{-1}$ interval) of corresponding $\Delta I(q)$ reported in part (**b**). Bottom: difference between the two $\Delta I(r)$ curves reported in the top part, equivalent to q-weighted FT of $\Delta[\Delta I(q)]$ bottom curve in part (**b**). The grey horizontal lines correspond to the zero on the y axis.

$\Delta[\Delta I(r)]$ intuitively represents the difference in electron density around the main scattering center, i.e. the Ru atom, as a function of inter-atomic distance r.[60] In the case of *cis*-$[Ru(bpy)_2(py)_2]^{2+}$, the Ru atom has the highest X-ray cross-section and thus $\Delta[\Delta I(r)]$ can picture bond cleavage or bond formation around the metal centre as negative and positive peaks, respectively.

As shown in Figure 4a, the experimental $\Delta[\Delta I(r)]$ curve (black circles) shows two well-defined negative peaks at 3.14 and 4.69 Å, and a shoulder around 2.50 Å. For *cis*-$[Ru(bpy)_2(py)_2]Cl_2$, the presence of these negative peaks is consistent with the movement of several

atoms of the molecule out of the Ru coordination sphere compared to their ground-state positions. In particular, the peaks at 3.14 and 4.69 Å suggest that TR-WAXS is able to detect, for the first time, the release of low Z atoms from the second and third shells.

In order to correctly assign each peak to the corresponding atoms of the released ligand, three TR-WAXS simulated curves were calculated using a simplified scattering model[62] and DFT-optimized structures of all the species involved in the photoprocess (Figure 4b).[63] In the first case the $\{[Ru(bpy)_2(py)]^{2+} + py\}$ and $[Ru(bpy)_2(py)_2]^{2+}$ structures (**M1**) were used to model the transient and the unperturbed complex, while in the second case the structures of the photoproducts $\{[Ru(bpy)_2(py)(H_2O)]^{2+} + py\}$ and the unperturbed system $\{[Ru(bpy)_2(py)_2]^{2+} + H_2O\}$ (**M2**) were employed, respectively. In the third model (**M3**), the structure of the photoproduct $[Ru(bpy)_2(py)(H_2O)]^{2+}$ was optimized by adding three explicit solvent molecules (water) H-bonded to the H_2O ligand coordinated to the Ru center. The **M3** strategy was aimed at determining a different photoproduct structure and assessing if a different Ru–O bond length, as well as solvent-cage effects, could result in a better simulated TR-WAXS curve. In our raw model the role of the counterion was neglected since the Ru–Cl distances are likely to be ≥ 5.5 Å and they do not change noticeably between laser-on and laser-off. Moreover, no coordination of Cl^- is observed for the aqueous solution of the complex at the end of prolonged light irradiation of the sample. An EXAFS experiment performed on an aqueous solution of *cis*-$[Ru(bpy)_2(py)_2]Cl_2$ confirmed the overall validity of the DFT structures, which nevertheless have Ru–N bond distances slightly overestimated. Comparison between the three simulated curves, **M1**–**M3**, and the experimental curve gives insights into the structural changes occurring to *cis*-$[Ru(bpy)_2(py)_2]Cl_2$ during the investigated photoreaction time-range (800 ns – 5.5 μs). Simulations confirm the dissociation of one pyridine ligand upon excitation. The well-defined negative peaks at 3.07–3.09 and 4.42–4.58 Å in **M1**–**M3** are in very good agreement with the loss of scattering signal observed in the experimental curve (peaks at 3.14 and 4.69 Å). Such negative peaks correspond to the contributions of the two *ortho* (3.07–3.09 Å) and two *meta* (4.42–4.58 Å) C atoms of the py (Figure 4b). The contribution of the *para* C atom at ca. 5 Å from the Ru is not well defined, due to the longer Ru–C distance (the signal decreases with a $1/r^2$ dependence) and to the presence of only a single C atom in this position.

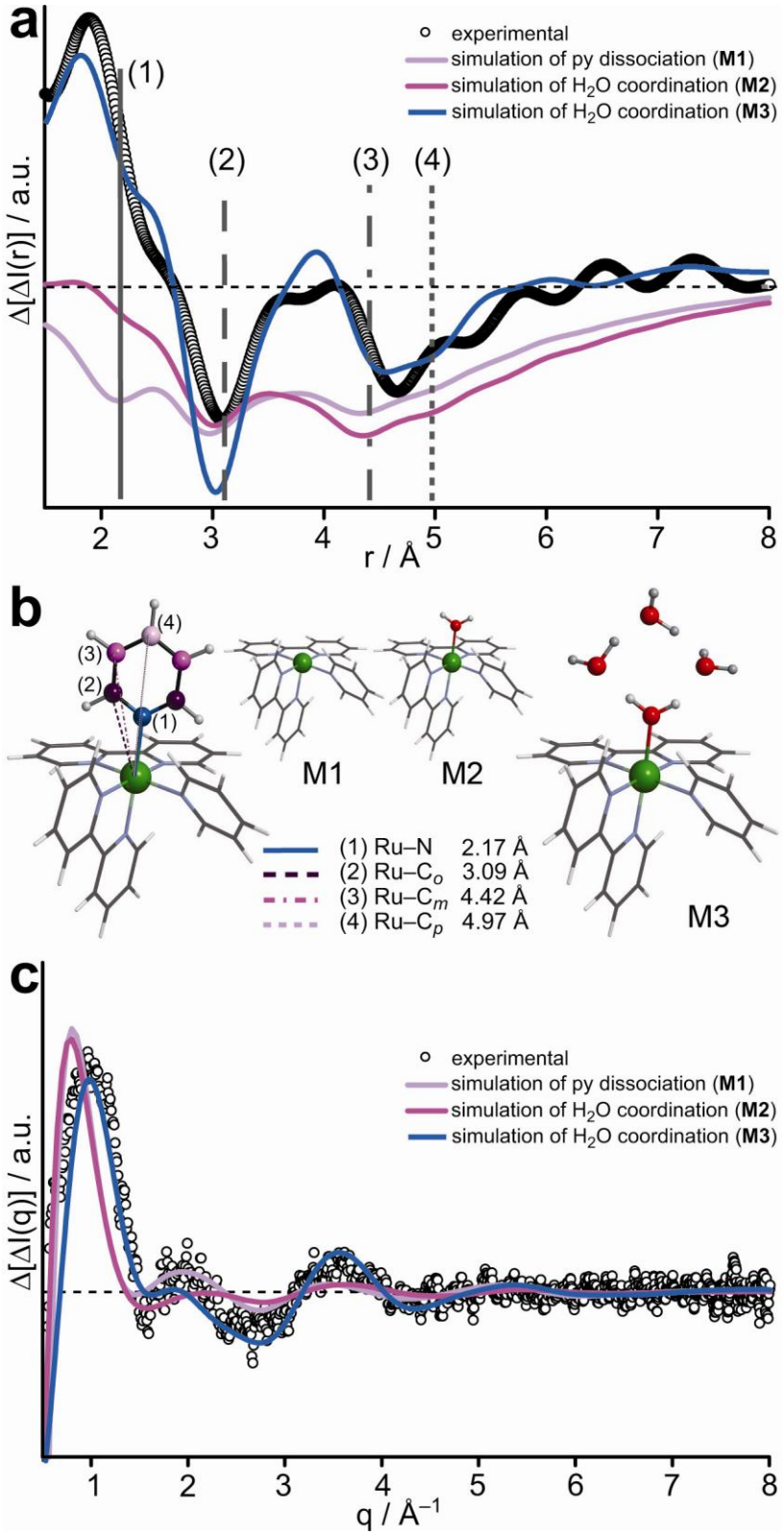

Figure 4. Interpretation of experimental Δ[ΔI(r)]. **a)** Experimental (black circles) and simulated (lilac = **M1**, pink = **M2** and light-blue = **M3**) Δ[ΔI(r)] curves. The three simulated curves are obtained using different models for the final photoproducts: for the lilac curve (**M1**) only the py dissociation is taken into account, i.e. $\{[Ru(bpy)_2(py)]^{2+} + py\}$, while for the pink (**M2**) and light-blue (**M3**) curve also the coordination of a water molecule is included, i.e. $\{[Ru(bpy)_2(py)(H_2O)]^{2+} + py\}$. All the structures employed in the simulations are obtained from DFT-optimized geometry calculations in water. In **M3**, the structure of the photoproduct *cis*-$[Ru(bpy)_2(py)(H_2O)]^{2+}$ was optimized by adding three explicit water molecules to simulate the solvent main effects (these three water molecules are included in the simulation of the TR-WAXS signal). Vertical bars are placed in correspondence of the Ru–N and Ru–C distances obtained from the DFT structure of *cis*-$[Ru(bpy)_2(py)_2]^{2+}$. **b)** Representation of DFT-optimized ground-state structure of

cis-$[Ru(bpy)_2(py)_2]^{2+}$, showing the distances where it is expected to observe a decrease in the radial distribution function upon pyridine ligand release by photodissociation; photoproduct modeling: $[Ru(bpy)_2(py)]^{2+}$ structure used in **M1** (from DFT-optimized structure of *cis*-$[Ru(bpy)_2(py)_2]^{2+}$**)** and DFT-optimized structures of $[Ru(bpy)_2(py)(H_2O)]^{2+}$ used in **M2** and **M3**. **c)** Experimental (black circles) and simulated (lilac = **M1**, pink = **M2** and light-blue = **M3**) Δ[ΔI(q)] curves.

In the 1.6–2.7 Å region, **M1** and the experimental curve differ significantly. Instead of the shoulder observed experimentally, **M1** has a negative peak which corresponds to the loss of the pyridine N atom (2.17 Å). This worse agreement between **M1** and the experimental curve in the 1.6–2.7 Å region is, in principle, unexpected as the experimental signal decreases as $1/r^2$. However, the **M2** simulation is able to clarify such result. In fact, when H_2O is included in the model structure of the photoproduct –replacement of the pyridine N atom with the almost isoelectronic O atom of a coordinated water molecule (Ru–O distance of 2.24 Å in the DFT optimized structure used for **M2**)– the simulated signal in the 1.6–2.7 Å region becomes a shoulder on the low-r side of the peak relative to the *ortho* C atoms. A further improvement in the simulation of the Δ[ΔI(r)] curve is obtained with **M3**. In this case, also the experimental positive peak at r = 1.95 Å is better reproduced, since **M3** shows a maximum at 1.87 Å.

The introduction of three water molecules H-bonded to the coordinated water significantly improves the agreement between the simulated curve **M3** and the experimental Δ[ΔI(r)], and this can be quantified/evaluated using the R factor, defined by eq. 1, where y_i is Δ[ΔI(r)] or Δ[ΔI(q)]. In the ideal case of a perfect agreement of the simulation with the experimental curve, the R factor is equal to zero.

$$R = \sqrt{\frac{\sum_i \left(y_i^{exp} - y_i^{sim}\right)^2}{\sum_i (y_i^{exp})^2}} \qquad \text{(eq. 1)}$$

The R factor obtained for **M3** is 0.31, while for **M1** and **M2** it is 1.37 and 1.41, respectively, indicating that **M3** better reproduces the global shape (position and relative intensity of the peaks) of the experimental Δ[ΔI(r)]. This trend is obviously observed also in the q-space (see Figure 4c); in this case the R factor for **M1**, **M2** and **M3** is 1.66, 1.03 and 0.57, respectively.

Despite the limitations due to the simplified model employed in the description of the X-ray scattering signal and the intrinsic errors in the DFT bond distances, the agreement between **M3** and the experimental curve indicates that *cis*-$[Ru(bpy)_2(py)_2]Cl_2$ dissociates the pyridine ligand and coordinate a solvent molecule within 800 ns of excitation. Furthermore, this result indicates that the O atom in the Ru–OH_2 bond of the photoproduct is at a shorter distance (Ru–O = 2.12 Å according to the DFT optimized structure used for **M3**) than the N atom in the Ru–N(py) bond of *cis*-$[Ru(bpy)_2(py)_2]Cl_2$ (Ru–N(py) = 2.17 Å).

Conclusions

Although limited by the excitation source and by the signal-to-noise ratio, the structural and temporal information obtained in this experiment are unique due to the relatively complex nature of the photoreleased ligand. Conversely, more is known on the femtosecond timescale of the photorelease of ligands such as CO.[33,64] On the basis of this first exciting result, future applications of TR-WAXS to photoactivatable metal anticancer agents can now be envisaged, including study of their photochemistry on shorter time-scales (1–100 ns), in biological conditions (e.g., salts, peptides, metabolites), and in the presence of target macromolecules relevant to tumor cells. Preliminary new data suggest that the time scale of the py photodissociation for *cis*-$[Ru(bpy)_2(py)_2]Cl_2$ is in the 100 ps–5 ns range (Supporting Information).

This work reports the first direct observation by TR-WAXS of light-induced ligand dissociation from a mononuclear metal complex in aqueous solution. Furthermore, to the best of our knowledge, this is the first successful application of this emerging technique to detect the release of a multiatomic fragment formed by low Z atoms. The experimental $\Delta[\Delta I(r)]$ curve shows features assignable to atoms not only in the first coordination shell of Ru, but also in the second and third shells as well. Detection of such a weak and highly structured signal opens up exciting prospects for the technique. Future advances could allow detailed TR-WAXS studies of the dynamics of photochemical processes under biologically- and catalytically-relevant conditions and involve characterization of three-dimensional reorientation of organic ligands around metal centers. A full treatment in the modeling of solvent-related terms for WAXS curves of such systems is required to achieve these challenging goals. Although difficult, addressing these aspects can lead to the full comprehension of the solvent behavior in photochemical processes involving metal complexes. This aspect of TR-WAXS gives complementary information with respect to TR-XAFS, which in contrast is atom-selective using the photoelectron as probe. This implies that TR-XAFS provides better evidence for differences in the first shell around the absorbing atom, whilst missing what happens at larger distances.

Summarizing, these findings have a wider significance in coordination chemistry. Ru^{II} is usually considered to be a relatively inert metal ion with ligand substitution reactions occurring on a ca. kilo-second or greater timescale (as is also the case for Ru^{III}). Whilst this is true for ground-state thermally-induced ligand substitution processes, it is evident that substitution reactions of excited states can take place on a micro-second or less timescale, a timescale usually associated with ligand substitution reactions of some first-row transition metals and s-block metals. Photoactivation therefore is potentially a very powerful additional strategy for varying the kinetic reactivity of metal ions.

Acknowledgements. L.S. was supported by a Marie Curie Intra European Fellowship 220281 (PHOTORUACD) within the 7th European Community Framework Programme, and by ERC grant 247450 (BIOINCMED to P.J.S). C.G. thanks Regione Piemonte for financial support. This experiment has been done in the frame of ESRF proposal CH-2719. Dr. S. Nikitenko (ESRF BM26) is acknowledged for the kind collection of EXAFS data.

Supporting Information Available: 1) laser pump and X-ray probe temporal width and relative delays; 2) complete EXAFS data analysis; 3) procedure for solvent scaling; 4) UV-Vis spectrum of *cis*-$[Ru(bpy)_2(py)_2]Cl_2$ in aqueous solution; 5) NMR spectra of *cis*-$[Ru(bpy)_2(py)_2]Cl_2$ before and after irradiation; 6) percentage estimation of photoreacted complex; 7) preliminary TR-WAXS data on the photodissociation process of *cis*-$[Ru(bpy)_2(py)_2]Cl_2$ in the 100 ps–5 ns time-range.

References and Notes

1. Murphy, C. J.; Arkin, M. R.; Jenkins, Y.; Ghatlia, N. D.; Bossmann, S. H.; Turro, N. J.; Barton, J. K., *Science* **1993,** *262*, 1025-1029.
2. Arkin, M. R.; Stemp, E. D. A.; Holmlin, R. E.; Barton, J. K.; Hormann, A.; Olson, E. J. C.; Barbara, P. F., *Science* **1996,** *273*, 475-480.
3. Erkkila, K. E.; Odom, D. T.; Barton, J. K., *Chem. Rev.* **1999,** *99*, 2777-2795.
4. Mackay, F. S.; Woods, J. A.; Heringova, P.; Kasparkova, J.; Pizarro, A. M.; Moggach, S. A.; Parsons, S.; Brabec, V.; Sadler, P. J., *Proc. Natl. Acad. Sci. U. S. A.* **2007,** *104*, 20743-20748.
5. Oregan, B.; Grätzel, M., *Nature* **1991,** *353*, 737-740.
6. Evans, R. C.; Douglas, P.; Winscom, C. J., *Coord. Chem. Rev.* **2006,** *250*, 2093-2126.
7. Chou, P. T.; Chi, Y., *Chem. Eur. J.* **2007,** *13*, 380-395.
8. Balzani, V.; Bergamini, G.; Marchioni, F.; Ceroni, P., *Coord. Chem. Rev.* **2006,** *250*, 1254-1266.
9. Fujita, E., *Coord. Chem. Rev.* **1999,** *185-6*, 373-384.
10. Salassa, L.; Garino, C.; Salassa, G.; Gobetto, R.; Nervi, C., *J. Am. Chem. Soc.* **2008,** *130*, 9590-9597.
11. Salassa, L.; Garino, C.; Salassa, G.; Nervi, C.; Gobetto, R.; Lamberti, C.; Gianolio, D.; Bizzarri, R.; Sadler, P. J., *Inorg. Chem.* **2009,** *48*, 1469-1481.
12. Betanzos-Lara, S.; Salassa, L.; Habtemariam, A.; Sadler, P. J., *Chem. Commun.* **2009**, 6622-6624.
13. Mahnken, R. E.; Billadeau, M. A.; Nikonowicz, E. P.; Morrison, H., *J. Am. Chem. Soc.* **1992,** *114*, 9253-9265.
14. Lutterman, D. A.; Fu, P. K. L.; Turro, C., *J. Am. Chem. Soc.* **2006,** *128*, 738-739.
15. Magennis, S. W.; Habtemariam, A.; Novakova, O.; Henry, J. B.; Meier, S.; Parsons, S.; Oswald, I. D. H.; Brabec, V.; Sadler, P. J., *Inorg. Chem.* **2007,** *46*, 5059-5068.
16. Mackay, F. S.; Farrer, N. J.; Salassa, L.; Tai, H. C.; Deeth, R. J.; Moggach, S. A.; Wood, P. A.; Parsons, S.; Sadler, P. J., *Dalton Trans.* **2009**, 2315-2325.
17. Aguirre, J. D.; Angeles-Boza, A. M.; Chouai, A.; Pellois, J. P.; Turro, C.; Dunbar, K. R., *J. Am. Chem. Soc.* **2009,** *131*, 11353-11360.
18. Farrer, N. J.; Salassa, L.; Sadler, P. J., *Dalton Trans.* **2009**, 10690-10701.
19. Salassa, L.; Phillips, H. I. A.; Sadler, P. J., *Phys. Chem. Chem. Phys.* **2009,** *11*, 10311-10316.
20. Chen, L. X.; Jäger, W. J. H.; Jennings, G.; Gosztola, D. J.; Munkholm, A.; Hessler, J. P., *Science* **2001,** *292*, 262-264.
21. Chen, L. X.; Shaw, G. B.; Novozhilova, I.; Liu, T.; Jennings, G.; Attenkofer, K.; Meyer, G. J.; Coppens, P., *J. Am. Chem. Soc.* **2003,** *125*, 7022-7034.
22. Bressler, C.; Chergui, M., *Chem. Rev.* **2004,** *104*, 1781-1812.
23. Zhang, X. Y.; Wasinger, E. C.; Muresan, A. Z.; Attenkofer, K.; Jennings, G.; Lindsey, J. S.; Chen, L. X., *J. Phys. Chem. A* **2007,** *111*, 11736-11742.
24. Chen, L. X.; Zhang, X. Y.; Wasinger, E. C.; Attenkofer, K.; Jennings, G.; Muresan, A. Z.; Lindsey, J. S., *J. Am. Chem. Soc.* **2007,** *129*, 9616-9618.

25. Chergui, M.; Zewail, A. H., *ChemPhysChem* **2009,** *10*, 28-43.
26. Bratos, S.; Mirloup, F.; Vuilleumier, R.; Wulff, M.; Plech, A., *Chem. Phys.* **2004,** *304*, 245-251.
27. Cammarata, M.; Levantino, M.; Schotte, F.; Anfinrud, P. A.; Ewald, F.; Choi, J.; Cupane, A.; Wulff, M.; Ihee, H., *Nat. Methods* **2008,** *5*, 881-886.
28. Lee, J. H.; Kim, J.; Cammarata, M.; Kong, Q.; Kim, K. H.; Choi, J.; Kim, T. K.; Wulff, M.; Ihee, H., *Angew. Chem.-Int. Edit.* **2008,** *47*, 1047-1050.
29. Kim, T. K.; Lorenc, M.; Lee, J. H.; Russo, M.; Kim, J.; Cammarata, M.; Kong, Q. Y.; Noel, S.; Plech, A.; Wulff, M.; Ihee, H., *Proc. Natl. Acad. Sci. U. S. A.* **2006,** *103*, 9410-9415.
30. Davidsson, J.; Poulsen, J.; Cammarata, M.; Georgiou, P.; Wouts, R.; Katona, G.; Jacobson, F.; Plech, A.; Wulff, M.; Nyman, G.; Neutze, R., *Phys. Rev. Lett.* **2005,** *94*, Art. n. 245503.
31. Ihee, H.; Lorenc, M.; Kim, T. K.; Kong, Q. Y.; Cammarata, M.; Lee, J. H.; Bratos, S.; Wulff, M., *Science* **2005,** *309*, 1223-1227.
32. Lee, J. H.; Kim, T. K.; Kim, J.; Kong, Q.; Cammarata, M.; Lorenc, M.; Wulff, M.; Ihee, H., *J. Am. Chem. Soc.* **2008,** *130*, 5834-5835.
33. Pinnick, D. V.; Durham, B., *Inorg. Chem.* **1984,** *23*, 1440-1445.
34. The term "shell" is used here as in EXAFS, to indicate the primary role of Ru-atom in the scattering process. In the WAXS technique all atoms of the system (solute and solvent molecules) contribute to the experimental signal, proportionally to their Z, and there is not a central absorber like in EXAFS. However, in the case of $[Ru(bpy)_2(py)_2]Cl_2$, the atomic pairs dominating the differential scattering signal include the pairs involving the high-Z Ru centre and one of the atom of the py ligand.
35. Dwyer, F. P.; Goodwin, H. A.; Gyarfas, E. C., *Aust. J. Chem.* **1963,** *16*, 544-548.
36. Frisch, M. J., Trucks, G. W., Schlegel, H. B., Scuseria, G. E., Robb, M. A., Cheeseman, J. R., Montgomery, J. A. Jr., Vreven, T., Kudin, K. N., Burant, J. C., Millam, J. M., Iyengar, S. S., Tomasi, J., Barone, V., Mennucci, B., Cossi, M, Scalmani, G., Rega, N., Petersson, G. A., Nakatsuji, H., Hada, M., Ehara, M., Toyota, K., Fukuda, R., Hasegawa, J., Ishida, M., Nakajima, T., Honda, Y., Kitao, O., Nakai, H., Klene, M., Li, X., Knox, J. E., Hratchian, H. P., Cross, J. B., Adamo, C., Jaramillo, J., Gomperts, R., Stratmann, R. E., Yazyev, O., Austin, A. J., Cammi, R., Pomelli, C., Ochterski, J., Ayala, P. Y., Morokuma, K., Voth, G. A., Salvador, P., Dannenberg, J. J., Zakrzewski, V. G., Dapprich, S., Daniels, A. D., Strain, M. C., Farkas, O., Malick, D. K., Rabuck, A. D., Raghavachari, K., Forestman, J. B, Ortiz, J. V., Cui, Q., Baboul, A. G., Clifford, S., Cioslowski, J., Stefanov, B. B, Liu, G., Liashenko, A., Piskorz, P., Komaromi, I., Martin, R. L., Fox, D. J., Keith, T., Al-Laham, M. A., Peng, C. Y., Nanayakkara, A., Challacombe, M., Gill, P. M. W., Johnson, B., Chen, W, Wong, M. W., Gonzales, C., Pople, J. A., *Gaussian 03* [revision D.01] **2004**, Wallingford CT, Gaussian Inc.
37. Becke, A. D., *J. Chem. Phys.* **1993,** *98*, 5648-5652.
38. Lee, C.; Yang, W.; Parr, R. G., *Phys. Rev. B: Condens. Matter* **1988,** *37*, 785-789.
39. Hay, P. J.; Wadt, W. R., *J. Chem. Phys.* **1985,** *82*, 270-283.
40. McLean, A. D.; Chandler, G. S., *J. Chem. Phys.* **1980,** *72*, 5639-5648.
41. Cossi, M.; Rega, N.; Scalmani, G.; Barone, V., *J. Comput. Chem.* **2003,** *24*, 669-681.
42. Cossi, M.; Barone, V., *J. Chem. Phys.* **2001,** *115*, 4708-4717.
43. Barone, V.; Cossi, M., *J. Phys. Chem. A* **1998,** *102*, 1995-2001.
44. Silversmit, G.; Vekemans, B.; Nikitenko, S.; Bras, W.; Czhech, V.; Zaray, G.; Szaloki, I.; Vincze, L., *J. Synchrot. Radiat.* **2009,** *16*, 237-246.
45. Ravel, B.; Newville, M., *J. Synchrot. Radiat.* **2005,** *12*, 537-541.
46. Ankudinov, A. L.; Nesvizhskii, A. I.; Rehr, J. J., *Phys. Rev. B* **2003,** *67*.
47. Salassa, L.; Gianolio, D.; Garino, C.; Salassa, G.; Borfecchia, E.; Ruiu, T.; Nervi, C.; Gobetto, R.; Bizzarri, R.; Sadler, P. J.; Lamberti, C., *J. Phys: Conf. Ser.* **2009,** *190*, Art. n. 012141.
48. Estephane, J.; Groppo, E.; Damin, A.; Vitillo, J. G.; Gianolio, D.; Lamberti, C.; Bordiga, S.; Prestipino, C.; Nikitenko, S.; Quadrelli, E. A.; Taoufik, M.; Basset, J. M.; Zecchina, A., *J. Phys. Chem. C* **2009,** *113*, 7305-7315.
49. Estephane, J.; Groppo, E.; Vitillo, J. G.; Damin, A.; Gianolio, D.; Lamberti, C.; Bordiga, S.; Quadrelli, E. A.; Basset, J. M.; Kervern, G.; Emsley, L.; Pintacuda, G.; Zecchina, A., *J. Phys. Chem. C* **2010,** *114*, 4451-4458.
50. Bonino, F.; Chavan, S.; Vitillo, J. G.; Groppo, E.; Agostini, G.; Lamberti, C.; Dietzel, P. D. C.; Prestipino, C.; Bordiga, S., *Chem. Mater.* **2008,** *20*, 4957-4968.
51. Chavan, S.; Vitillo, J. G.; Groppo, E.; Bonino, F.; Lamberti, C.; Dietzel, P. D. C.; Bordiga, S., *J. Phys. Chem. C* **2009,** *113*, 3292-3299.
52. Cavka, J. H.; Jakobsen, S.; Olsbye, U.; Guillou, N.; Lamberti, C.; Bordiga, S.; Lillerud, K. P., *J. Am. Chem. Soc.* **2008,** *130*, 13850-13851.
53. Wulff, M.; Plech, A.; Eybert, L.; Randler, R.; Schotte, F.; Anfinrud, P., *Faraday Discuss.* **2002,** *122*, 13-26.
54. Jackson, J. D., *Classical electrodynamics*. 3rd ed.; New York, 1999.
55. Head-Gordon, T.; Hura, G., *Chem. Rev.* **2002,** *102*, 2651-2669.
56. Plech, A.; Randler, R.; Armin, G.; Wulff, M., *J. Synchrot. Radiat.* **2002,** *9*, 287-292.
57. Kim, T. K.; Lee, J. H.; Wulff, M.; Kong, Q. Y.; Ihee, H., *ChemPhysChem* **2009,** *10*, 1958-1980.

58. Wacholtz, W. M.; Auerbach, R. A.; Schmehl, R. H.; Ollino, M.; Cherry, W. R., *Inorg. Chem.* **1985,** *24*, 1758-1760.
59. Adelt, M.; Devenney, M.; Meyer, T. J.; Thompson, D. W.; Treadway, J. A., *Inorg. Chem.* **1998,** *37*, 2616-2617.
60. Ihee, H., *Acc. Chem. Res.* **2009,** *42*, 356-366.
61. Fader, W. J., *J. Appl. Phys.* **1976,** *47*, 1975-1978.
62. The simulated $\Delta[\Delta I(r)]$ curves are obtained Fourier-transforming the q-dependent scattered intensities $\Delta[\Delta I(q)]$ curves calculated solving the Debye equation for the molecular fragments involved in the photoprocess. Debye equation includes only isolated solute molecules in the gas phase and neglects effects due to rearrangement of the solute molecules in the solvation shell. Although a more sophisticated modeling of the solute-solvent interaction (Molecular Dynamics) can improve the fitting of experimental data, we show here that the raw Debye model can fully describe the photochemical process of *cis*-$[Ru(bpy)_2(py)_2]Cl_2$. The effect of the slightly asymmetric X-ray spectrum from the undulator beam (U17, E_f = 18,25 keV, 3% BW), resulting in a small q-broadening and peak shift, was taken into account in all simulated curves. For details see Ref. [53].
63. Lee, J. H.; Kim, K. H.; Kim, T. K.; Lee, Y.; Ihee, H., *J. Chem. Phys.* **2006,** *125*, Art. n. 174504
64. Gabrielsson, A.; Záliš, S.; Matousek, P.; Towrie, M.; Vlček, A., *Inorg. Chem.* **2004,** *43*, 7380-7388.

Figure for the TOC

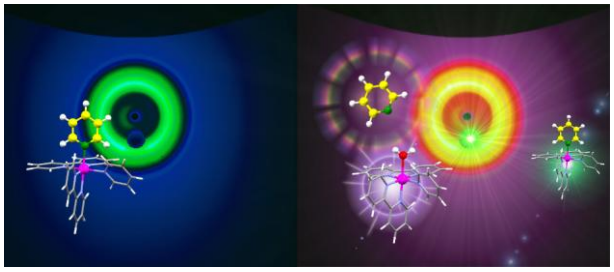

Time-Resolved Wide Angle X-ray Scattering is successfully employed to study the photochemistry of *cis*-$[Ru(bpy)_2(py)_2]Cl_2$. This technique is able to directly capture the structural changes in the metal complex due to the release of a pyridine ligand and the coordination of a solvent molecule within 800 ns of laser excitation.